Supplementary Information for Microwave Mode Cooling and Cavity Quantum Electrodynamics Effects at Room Temperature with Optically Cooled Nitrogen-Vacancy Center Spins

Yuan Zhang,[1,*] Qilong Wu,[1] Hao Wu,[2,3] Xun Yang,[1] Shi-Lei Su,[1] Chongxin Shan,[1,†] and Klaus Mølmer[4,5,‡]

[1] *Henan Key Laboratory of Diamond Optoelectronic Materials and Devices, Key Laboratory of Material Physics, Ministry of Education, School of Physics and Microelectronics, Zhengzhou University, Daxue Road 75, Zhengzhou 450052 China*

[2] *Center for Quantum Technology Research and Key Laboratory of Advanced Optoelectronic Quantum Architecture and Measurements (MOE), School of Physics, Beijing Institute of Technology, Beijing 100081, China*

[3] *Beijing Academy of Quantum Information Sciences, Beijing 100193, China*

[4] *Center for Complex Quantum Systems, Department of Physics and Astronomy, Aarhus University, Ny Munkegade 120, DK-8000 Aarhus C, Denmark*

[5] *Aarhus Institute of Advanced Studies, Aarhus University, Høegh-Guldbergs Gade 6B, DK-8000 Aarhus C, Denmark*

SUPPLEMENTARY NOTE 1: PARAMETERS FOR THE SIMULATIONS IN THE MAIN TEXT

In the Supplementary Table 1, we present the parameters applied in the simulations of the main text, where the upper part is from the microwave mode cooling experiment [1] and the lower part is mainly from the diamond maser experiment [2]. Here, we assume the relatively smaller Zeeman shift induced by a relatively weak magnetic field so that the $+1 \rightarrow 0$ spin level transition couples resonantly with the microwave resonator.

According to the experiment [1], the optical pumping rate ξ can be calculated with the following expression

$$\xi = \frac{\lambda_P \sigma_{\lambda_P}}{hcA_p l\alpha}\left(1-e^{-l\alpha}\right)(1-R)\,P. \tag{1}$$

Here, $\sigma_{\lambda_p} = 3.1\times10^{-21}\mathrm{m}^2$ is the absorption cross-section of the NV centers at the laser wavelength $\lambda_p = 532$ nm. $h = 6.63\times10^{-34}$ J $\cdot$ s is the Planck constant, $c = 2.99\times10^{8}$ m/s is the speed of light. $A_p = 1.76\times10^{-6}$ m^2 is the cross-sectional area of the pump beam on the sample. $l = 1.5$ mm is the thickness of the diamond crystal. $\alpha = 2.3\times10^{3}$ m^{-1} is the absorption coefficient at λ_P. $R = \left|\frac{n_1-n_2}{n_1+n_2}\right|^2$ is Fresnel reflection coefficient with the refractive index of air $n_1 = 1$ and of the diamond $n_2 = 2.42$. P is the laser power in unit of W. These parameters are estimated for the setup in Ref. [1], and might vary for the proposed setup. In any case, we expect that these values might lead to a reasonable estimation of the optical pumping rate for given laser power.

It is worth noting that by optimizing the system setup, such as absorption of the diamond with a tapered configuration [3] or total reflection [4], the optical pumping rate ξ might be increased by one to two orders of magnitude for the same laser power. Furthermore, the typical commercial CW solid-state laser of 532 nm can provide powers up to 20 W, and the pulsed solid-state laser can provide peak powers up to 100 W or even 1000 W.

For the performance of the microwave mode cooling and the CQED effects, the spin-lattice relaxation rate, the spin dephasing rate and the number of NV spins are the three key parameters. At room temperature, the former rate is determined by two-phonon Raman process and Orbach-type process, and seems to be consistent among different samples [5]. However, this rate is sensitive to the applied magnetic field, and shows resonant feature with about ten times larger value at the magnetic field of about 51, 102 mT, because of the resonant coupling of the electron spin levels with the nuclear spin levels [6–8]. However, by departing from these conditions, the spin-lattice relaxation rate is in the order of hundreds Hertz, as considered in the experiment [2].

The spin dephasing rate is determined by the decoherence time T_2^* for the nitrogen-rich diamond. In return, T_2^* is mainly determined by the paramagnetic substitutional nitrogen defects $\mathrm{N_S^0}$ (also known as P1 centers), and is inversely proportional to the defect concentration $[\mathrm{N_S^0}]$ in unit ppm: $1/T_2^* \approx A_{\mathrm{N_S^0}}[\mathrm{N_S^0}]$ with the coefficient $A_{\mathrm{N_S^0}} = 101$ $\mathrm{ms^{-1}ppm^{-1}}$ [9]. In the diamond maser experiment [2], the P1 center concentration is estimated as $[\mathrm{N_S^0}] \approx 4$ ppm and

* yzhuaudipc@zzu.edu.cn
† cxshan@zzu.edu.cn
‡ moelmer@phys.au.dk

Description	Symbol	Value
Transition rates between NV multiple levels [1]		
Optical pumping and decay rate	ξ	$0-1$ MHz
Spontaneous emission rate	k_{sp}	66 MHz
Inter-system crossing rates	k_{47}	7.9 MHz
	$k_{67}=k_{57}$	53 MHz
	$k_{73}=k_{72}$	0.73 MHz
	k_{71}	1.0 MHz
Parameters related to the diamond maser experiment [2]		
Resonator Frequency	ω_c	$2\pi\times 9.22$ GHz
Photon damping rate	κ	1.88 MHz
Spin-resonator coupling	g_{31}	0.69 Hz
Number of spins	N	4×10^{13}
Spin level transition frequency	ω_{31}	$2\pi\times 9.22$ GHz
	ω_{12}	$2\pi\times 3.48$ GHz
Spin dephasing rate	$\chi_2=\chi_3$	$2\pi\times 0.64$ MHz
Spin-lattice relaxation rate	$k_{31}\approx k_{12}$	208 Hz

Supplementary Table 1. **System parameters.** Parameters for the dissipation rates of NV centers (upper part), as reported [1], and the parameters for the microwave resonator and NV spins, as reported in the diamond maser experiment [2]. In our proposed setup, the $+1\rightarrow 0$ spin transition with frequency ω_{31} couples resonantly to the microwave resonator mode.

the decoherence time is evaluated as $T_2^*\approx 2.48$ μs, about five times longer than the measured value 0.5 μs. Since the scaling coefficient $A_{\mathrm{N_S^0}}$ can have a discrepancy of ten times in different theoretical simulations, the discrepancy here is not surprised. In our simulations, we utilize the reported dephasing rate $2/T_2^*\approx 4$ MHz.

Besides the spin-dephasing rate, the number of the negatively charged nitrogen-vacancy ($\mathrm{NV^-}$) centers is also important. Thus, the product $[\mathrm{NV^-}]T_2^*$ of the $\mathrm{NV^-}$ concentration $[\mathrm{NV^-}]$ and the decoherence time T_2^* should be considered when optimizing the system performance. Approximating $[\mathrm{NV^-}]$ with $[\mathrm{N_S^0}]$, we should look at the product $[\mathrm{N_S^0}]T_2^*$. According to Ref. [10], this product saturates for $[\mathrm{N_S^0}]$ larger than 1 ppm for the diamond sample with neutral abundant ^{13}C (1.1%), but starts saturating only for $[\mathrm{N_S^0}]$ larger than 40 ppm for the diamond sample with depleted ^{13}C (0.005%). The diamond sample, as used in the experiment [2] and considered here, is already in the range of saturation. However, the property might be improved by several times if the sample with depleted ^{13}C is used.

a

```
using QuantumCumulants;
@cnumbers N Δω31 ξ ksp k47 k57 k67 k73 k72 k71 k31 k13 k21 k12 χ2 χ3;
@cnumbers Δωm g31 κ nmth Ω ωd;
hm = FockSpace(:resonator);
hNV_ = NLevelSpace(:NV,7) ;
hNV = ClusterSpace(hNV_, N, 2) ;
h = hm⊗ hNV;
@qnumbers a::Destroy(h);
σ(i,j) = Transition(h, :σ, i, j, 2);
H = Δω31*sum(σ(3,3)) + Δωm*a'a + g31*(a'*sum(σ(1,3)) + a*sum(σ(3,1)))+ Ω*(a' + a);
J = [σ(4,1),σ(5,2),σ(6,3),σ(1,4),σ(2,5),σ(3,6), σ(7,4),σ(7,5),σ(7,6),σ(2,7),σ(3,7),σ(1,7), σ(1,2),σ(1,3),σ(2,1),σ(3,1),σ(2,2),σ(3,3), a,a'];
rates = [ξ,ξ,ξ,ξ+ksp,ξ+ksp,ξ+ksp,k47,k57,k67,k72,k73, k71, k21,k31,k12,k13,2*χ2,2*χ3,(1.0+nmth)*κ, nmth* κ];
ops =[a'*a,σ(2,2)[1],σ(3,3)[1]];
eqs = meanfield(ops, H, J;rates=rates, order=2);
eqs_c = complete(eqs, order=2);
```

b

```
N_ = 4e14; ksp_ = 6.6e7; k47_ = 7.9e6;k57_ = 5.3e7;k67_ = 5.3e7; k73_ = 7.3e5; k72_ = 7.3e5;k71_ = 1.0e6;ω31__ = 2*pi*9.22e9; k13_=k31_=k21_ =k12_=208; χ2_ = 2*pi*0.64e6; χ3_ = 2*pi*0.64e6;
λp = 532e-9; σλp = 3.1e-21; c = 2.99792458e8; Ap = 1.76e-6; l = 1.5e-3; α = 2.3e3; n_1 = 1; n_2 = 2.42; R = abs((n_1-n_2)/(n_1+n_2))^2;P = 1;ξ_ = (λp*σλp)/(hh*c*Ap*l*α)*(1-exp(-l*α))*(1-R)*P;
ωm_ = 2*pi*9.22e9; nmth_ = 1.0/(exp(hbar*ωm_/ kbT)-1);g31_ = 2*pi*0.11; κ_ = 2*pi*0.8e6; Δωm_=0; Δω31 _=0;
ps = [N, Δ ω31,ξ,ksp,k47,k57,k67,k73,k72,k71,k31,k13,k21, k12,χ2,χ3, Δ ωm,g31,κ,nmth];
p0 = [N_, Δω31_,ξ_,ksp_,k47_,k57_,k67_,k73_,k72_, k71_,k31_,k13_,k21_,k12_,χ2_,χ3_, Δωm_,g31_,κ_,nmth_];
u0 = zeros(ComplexF64, length(eqs_c)); u0[1] = nmth_; u0[2] = 1.0/(1.0+k21_/k12_*(1.0+k13_/k31_)); u0[3] = 1.0/(1.0+k31_/k13_*(1.0+k12_/k21_));
using OrdinaryDiffEq, ModelingToolkit
sys = ODESystem(eqs_c);
prob0 = ODEProblem(sys,u0,(0.0, 20e-3), ps.=>p0);
sol0 = solve(prob0,RK4());
t0 = sol0.t;n0 = real.(sol0[sys.states[1]]);p20 = real.(sol0[sys.states[2]]); p30 = real.(sol0[sys.states[3]]); p40 = real.(sol0[sys.states[4]]); p50 = real.(sol0[sys.states[5]]); p60 = real.(sol0[sys.states[6]]); p70 = real.(sol0[sys.states[7]]); p10 = 1.0 - (p20 + p30 + p40 + p50 + p60 + p70);
se = p30/(p30+p10);
smsp = sol0[sys.states[16]]
sese = sol0[sys.states[47]]/(p30+p10)^2;
szsz = 4*sese.-4*se.+ 1;
M = real.(se).-0.5; J = real.(sqrt.(0.75/N_.+((N_ -1)/N_)*(smsp.+0.25*szsz)));
using Plots;
plot(t0/1e-3, n0, xlabel="time (ms)", ylabel="⟨a⁺a⟩");
plot(t0/1e-3, p20, xlabel="time (ms)", ylabel="⟨σ22⟩");
plot(t0/1e-3, p30, xlabel="time (ms)", ylabel="⟨σ33⟩");
plot(J, M);
```

Supplementary Figure 1. **Julia codes to derive the mean-field equations (a) and to solve the equations (b)**.

SUPPLEMENTARY NOTE 2: JULIA CODES TO DERIVE AND SOLVE MEAN-FIELD EQUATIONS

In this Supplementary Note, we present the Julia codes to derive the mean-field equations (Supplementary Figure 1a) and to solve these equations (Supplementary Figure 1b). First, we explain the former code. The 1st line imports the QuantumCumulants.jl package, and the 2nd and 3rd lines define the complex numbers. Here, we work in a frame rotating with the microwave driving field frequency ω_d and introduce the frequency detuning $\Delta\omega_{31} = \omega_{31} - \omega_d$ and $\Delta\omega_m = \omega_m - \omega_d$. The 4th line defines the Hilbert space of the microwave resonator as a quantized harmonic oscillator, while the 5th line defines that of the single NV center as a seven-levels system. The 6th line defines the Hilbert space of the N NV centers, where the last argument indicates the number of representative NV centers labeled by $k = 1, 2$, and the 7th line defines the Hilbert space of the NV centers-microwave resonator system. The 8th line defines the annihilation operator of the microwave photons, and the 9th line defines the projection operators $\sigma(i,i) = \left\{\hat{\sigma}_1^{ii}, \hat{\sigma}_2^{ii}\right\}$ with $i = 1, ..., 7$ and the transition operators $\sigma(i,j) = \left\{\hat{\sigma}_1^{ij}, \hat{\sigma}_2^{ij}\right\}$ with $i \neq j$. The 10th line defines the system Hamiltonian, while the 11th and 12th line define the list of operators and values to specify the Lindblad super-operators. The 13th line defines a list of three operators, and the 14th line derives the equations for the expectation value of these operators. The 15th line analyzes the unknown mean-field quantities, and derives the equations for them to form a closed set of equations, see the Supplementary Note 3 for an example. In the derivation, we have assumed vanishing third-order cumulant to approximate $\langle\hat{o}\hat{p}\hat{q}\rangle$ as $\langle\hat{o}\rangle\langle\hat{p}\hat{q}\rangle + \langle\hat{p}\rangle\langle\hat{o}\hat{q}\rangle + \langle\hat{q}\rangle\langle\hat{o}\hat{p}\rangle - 2\langle\hat{o}\rangle\langle\hat{p}\rangle\langle\hat{q}\rangle$ for any operators $\hat{o}, \hat{p}, \hat{q}$.

Second, we describe the code to solve the equations, see the Supplementary Figure 1b. The 1st line specifies the parameters related to the NV centers, and the 2nd line calculates the optical pumping rate for the laser excitation with the reference power 1 W. The 3rd line specifies the parameters related to the microwave resonator. The 4th and 5th line define the list of the symbols and of their values. The 6th line defines the initial conditions for the unknown mean-field quantities. The 7th line imports the "OrdinaryDiffEq" and "ModelingToolkit" packages to define and solve the ordinary differential equations (ODE). The 8th line defines the ODE system with the derived mean-field equations, and the 9th line defines the ODE problem with the initial condition, the time argument and the parameters. The 10th line solves the ODE with Rounge-Kutta method, and the 11th line extracts the list of simulation time and the physical quantities of interest. The 12th line calculates the relative population, and the 13-15th lines calculate the spin-spin correlations. The 16th line calculates the Dicke state quantum number J, M. The 17th line imports the "Plots" package, and the remaining lines plot the dynamics of the mean photon number, the levels population, and the Dicke states.

We use the Dicke state quantum numbers J, M to represent the quantum state of the NV center ensemble. M can be calculated as $M/N = \left\langle\hat{\sigma}_1^{33}\right\rangle / (\left\langle\hat{\sigma}_1^{33}\right\rangle + \left\langle\hat{\sigma}_1^{11}\right\rangle) - 0.5$, where $\left\langle\hat{\sigma}_1^{11}\right\rangle$ and $\left\langle\hat{\sigma}_1^{33}\right\rangle$ are the population of the 1st and 3nd ($m_s = 0, 1$) spin levels, respectively. J can be computed as $J/N = \sqrt{\frac{3}{4N} + \frac{N-1}{N}(\langle\hat{\sigma}_1^{13}\hat{\sigma}_2^{31}\rangle + \frac{1}{4}\langle\hat{\sigma}_1^z\hat{\sigma}_2^z\rangle)}$ with $\langle\hat{\sigma}_1^z\hat{\sigma}_2^z\rangle = 4\left\langle\hat{\sigma}_1^{33}\hat{\sigma}_2^{33}\right\rangle - 4\left\langle\hat{\sigma}_1^{33}\right\rangle / (\left\langle\hat{\sigma}_1^{33}\right\rangle + \left\langle\hat{\sigma}_1^{11}\right\rangle) + 1$, where $\langle\hat{\sigma}_1^z\hat{\sigma}_2^z\rangle, \left\langle\hat{\sigma}_1^{33}\hat{\sigma}_2^{33}\right\rangle, \left\langle\hat{\sigma}_1^{13}\hat{\sigma}_2^{31}\right\rangle$ are the spin-spin correlations.

SUPPLEMENTARY NOTE 3: CLOSED SET OF SECOND-ORDER MEAN-FIELD EQUATIONS FOR MICROWAVE MODE COOLING

In this Supplementary Note, we show the closed set of derived mean-field equations in second order. Here, we focus on the microwave mode cooling, and do not include the microwave field driving. First, we present the equations for the first-order mean-field quantities. The population $\langle\hat{\sigma}_1^{ii}\rangle$ of various levels of NV centers follows the equations

$$\partial_t\langle\hat{\sigma}_1^{11}\rangle = -(k_{12}+k_{13}+\xi)\langle\hat{\sigma}_1^{11}\rangle + (\xi+k_{sp})\langle\hat{\sigma}_1^{44}\rangle + k_{21}\langle\hat{\sigma}_1^{22}\rangle + k_{31}\langle\hat{\sigma}_1^{33}\rangle - ig_{31}\left(\langle\hat{a}^\dagger\hat{\sigma}_1^{13}\rangle - \langle\hat{a}\hat{\sigma}_1^{31}\rangle\right), \tag{2}$$

$$\partial_t\langle\hat{\sigma}_1^{22}\rangle = -\xi\langle\hat{\sigma}_1^{22}\rangle + (k_{sp}+\xi)\langle\hat{\sigma}_1^{55}\rangle + k_{72}\langle\hat{\sigma}_1^{77}\rangle + k_{12}\langle\hat{\sigma}_1^{11}\rangle - k_{21}\langle\hat{\sigma}_1^{22}\rangle, \tag{3}$$

$$\partial_t\langle\hat{\sigma}_1^{33}\rangle = -\xi\langle\hat{\sigma}_1^{33}\rangle + (k_{sp}+\xi)\langle\hat{\sigma}_1^{66}\rangle + k_{73}\langle\hat{\sigma}_1^{77}\rangle + k_{13}\langle\hat{\sigma}_1^{11}\rangle - k_{31}\langle\hat{\sigma}_1^{33}\rangle + ig_{31}\left(\langle\hat{a}^\dagger\hat{\sigma}_1^{13}\rangle - \langle\hat{a}\hat{\sigma}_1^{31}\rangle\right), \tag{4}$$

$$\partial_t\langle\hat{\sigma}_1^{44}\rangle = \xi\langle\hat{\sigma}_1^{11}\rangle - (k_{sp}+\xi)\langle\hat{\sigma}_1^{44}\rangle - k_{47}\langle\hat{\sigma}_1^{44}\rangle, \tag{5}$$

$$\partial_t\langle\hat{\sigma}_1^{55}\rangle = \xi\langle\hat{\sigma}_1^{22}\rangle - (\xi+k_{sp})\langle\hat{\sigma}_1^{55}\rangle - k_{57}\langle\hat{\sigma}_1^{55}\rangle, \tag{6}$$

$$\partial_t\langle\hat{\sigma}_1^{66}\rangle = \xi\langle\hat{\sigma}_1^{33}\rangle - (\xi+k_{sp})\langle\hat{\sigma}_1^{66}\rangle - k_{67}\langle\hat{\sigma}_1^{66}\rangle, \tag{7}$$

$$\partial_t\langle\hat{\sigma}_1^{77}\rangle = k_{47}\langle\hat{\sigma}_1^{44}\rangle + k_{57}\langle\hat{\sigma}_1^{55} + k_{67}\langle\hat{\sigma}_1^{66}\rangle - (k_{71}+k_{72}+k_{73})\langle\hat{\sigma}_1^{77}\rangle. \tag{8}$$

Second, we illustrate the equations for the second-order mean values. The mean intra-resonator photon number $\langle\hat{a}^\dagger\hat{a}\rangle$ satisfies the equation

$$\partial_t\langle\hat{a}^\dagger\hat{a}\rangle = \kappa\left(n_m^{th} - \langle\hat{a}^\dagger\hat{a}\rangle\right) + iNg_{31}\left(\langle\hat{a}\hat{\sigma}_1^{31}\rangle - \langle\hat{a}^\dagger\hat{\sigma}_1^{13}\rangle\right). \tag{9}$$

Frequency	$\omega_c = 2\pi f_c$	$2\pi \times 2.872$ GHz
Quality-factor	$Q = f_c/\kappa$	2900
Damping rate	κ	6.22 MHz
Spin-resonator coupling	g_{31}	0.084 Hz
Number of spins	N	1.6×10^{15}
Spin transition frequency	ω_{31}	$2\pi \times 2.872$ GHz
	ω_{21}	$2\pi \times 2.867$ GHz
Spin-lattice relaxation rate	$k_{31} \approx k_{12}$	83 Hz
Spin dephasing rate	$\chi_2 = \chi_3$	$2\pi \times 2.6$ MHz

Supplementary Table 2. **Parameters related to the microwave mode cooling experiments [1].**

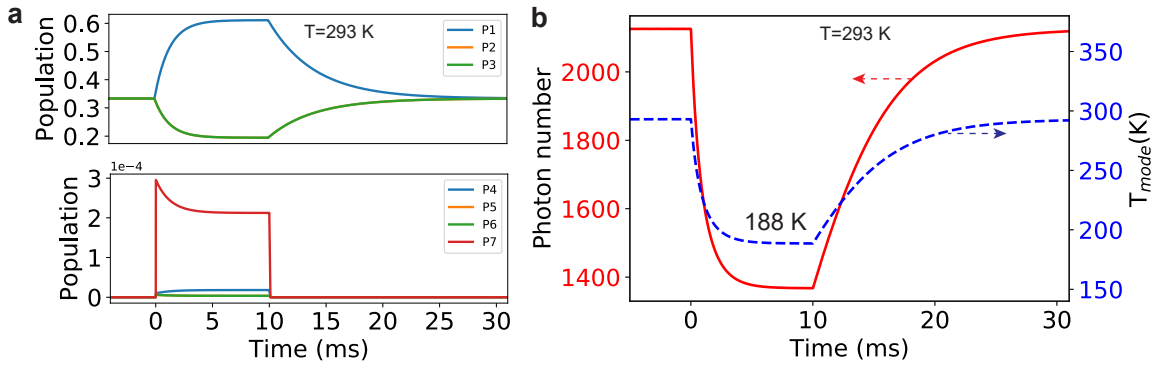

Supplementary Figure 2. **Cooling dynamics of a NV spin ensemble and a microwave resonator mode.** Similar results as those in Fig. 2 in the main text, but for the a low frequency microwave resonator as used in the microwave mode cooling experiment [1].

The NV-photon correlation $\langle \hat{a}^\dagger \hat{\sigma}_1^{13} \rangle$ follows the equation

$$\begin{aligned} \partial_t \langle \hat{a}^\dagger \hat{\sigma}_1^{13} \rangle &= i\left(\omega_m - \omega_{31}\right) \langle \hat{a}^\dagger \hat{\sigma}_1^{13} \rangle - \left[\left(\kappa + k_{12} + k_{13} + k_{31}\right)/2 + \xi + \chi_3\right] \langle \hat{a}^\dagger \hat{\sigma}_1^{13} \rangle \\ &+ i g_{31} \left[\langle \hat{\sigma}_1^{33} \rangle \left(1 + \langle \hat{a}^\dagger \hat{a} \rangle\right) - \langle \hat{\sigma}_1^{11} \rangle \langle \hat{a}^\dagger \hat{a} \rangle\right] + i(N-1) g_{31} \langle \hat{\sigma}_1^{31} \hat{\sigma}_2^{13} \rangle. \end{aligned} \tag{10}$$

The correlations $\langle \hat{a} \hat{\sigma}_1^{31} \rangle$ are simply the complex conjugation of $\langle \hat{a}^\dagger \hat{\sigma}_1^{13} \rangle$. In the end, the NV-NV correlation $\langle \hat{\sigma}_1^{31} \hat{\sigma}_2^{13} \rangle$ satisfies the equation

$$\partial_t \langle \hat{\sigma}_1^{31} \hat{\sigma}_2^{13} \rangle = -\left[k_{12} + k_{13} + k_{31} + 2\left(\xi + \chi_3\right)\right] \langle \hat{\sigma}_1^{31} \hat{\sigma}_2^{13} \rangle + i g_{31} \left(\langle \hat{\sigma}_1^{33} \rangle - \langle \hat{\sigma}_1^{11} \rangle\right) \left(\langle \hat{a} \hat{\sigma}_1^{31} \rangle - \langle \hat{a}^\dagger \hat{\sigma}_1^{13} \rangle\right). \tag{11}$$

SUPPLEMENTARY NOTE 4: MICROWAVE MODE COOLING WITH A LOWER FREQUENCY RESONATOR

In this Supplementary Note, we present results similar to those in the main text but for the setup used in the microwave mode cooling experiment [1], which features a microwave resonator with lower frequency. In the Supplementary Table 2, we present the parameters applied in the simulations. Here, we assume a spin dephasing rate $2\pi \times 2.6$ MHz, which is consistent with the value reported in experiments at low temperature [11, 12], but an order of magnitude larger than 0.33 MHz as assumed in the experiment [1]. The latter value is obtained by assuming that the NV^- concentration is equal to that of the P1 centers, while usually the P1 centers concentration can be orders of magnitude larger [13]. We note that our conservative value is also of the same order of magnitude as the width of the zero-field transient electron paramagnetic resonance measurement, see Fig. 2b in [1].

With the transition rates in the upper part of the Supplementary Table 1 and the parameters in the Supplementary Table 2, we have simulated the cooling dynamics (Supplementary Figure 2) and steady-state (Supplementary Figure 3) of the NV centers and the coupled microwave resonator. Supplementary Figure 2 shows similar results as Fig. 2 in the main text except: (1) the intra-resonator photon number starts from relatively larger thermal value 2125 because

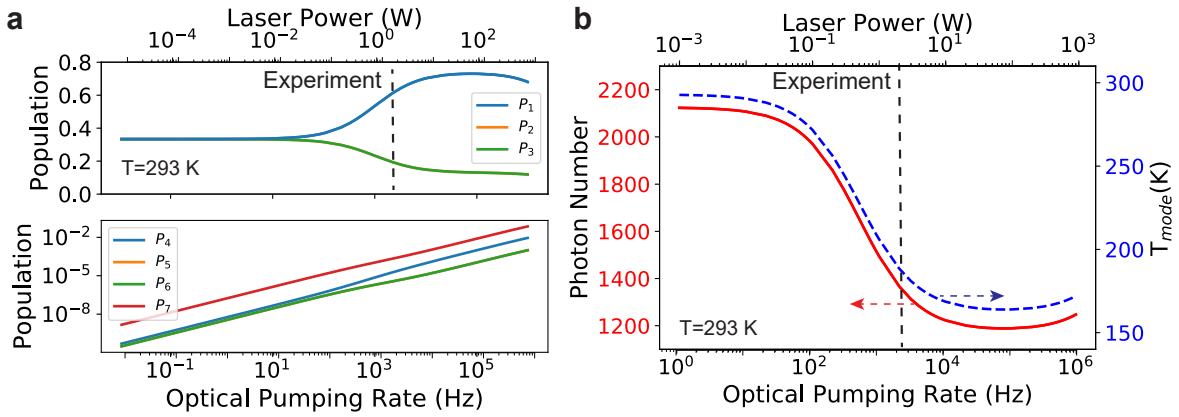

Supplementary Figure 3. **Steady-state cooling of the NV spins and the microwave resonator mode.** Similar results as those in Fig. 3 in the main text but for the low frequency microwave resonator as used in the microwave mode cooling experiment [1].

the single photon energy $\hbar\omega_m$ is much smaller than the thermal energy k_BT; (2) the effective mode temperature reduces to 188 K, about 35 K higher than 153 K in Fig. 2b of the main text, due to the insufficient energy transfer from the NV centers to the microwave mode. Supplementary Figure 3 shows similar results as Fig. 3 in the main text except that the minimal mode temperature is 170 K, about 54 K higher than the value 116 K in Fig. 3b. The dynamics of the mode temperature reproduces the experimental results [1], and the mode temperature can be reduced from 188 K to the minimal temperature 170 K by increasing the laser power from 2 W to 100 W. In addition, we verify that the rate equations given in the Supplementary Note 5 can reproduce perfectly the results, because the system works in the weak coupling regime, and the spin-spin correlation does not play a role here.

For the current setup, we estimate the largest NV spins-microwave mode coupling as $\sqrt{2J}g \approx 2\pi \times 0.45$ MHz, and conclude that the system is in the weak collective coupling regime since this coupling is much smaller than the spin dephasing rate $\chi_3 = 2\pi \times 2.6$ MHz. As a result, with this setup, we do not expect to realize C-QED effects at room temperature.

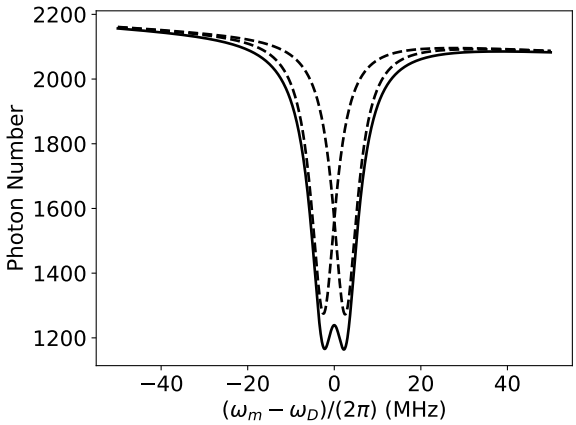

Supplementary Figure 4. **Influence of two NV spin transitions on the microwave mode cooling.** Intra-resonator steady-state photon number as a function of the detuning of the microwave mode frequency ω_m to the middle frequency $\omega_D = (\omega_{31} + \omega_{21})/2$ of the $0 \to +1$ and $0 \to -1$ transitions, for the laser excitation with 2 W power. The dashed lines indicate the results when only one transition is considered.

Considering the large spin-dephasing rate, the -1 spin level might also influence the microwave mode cooling even though it is off-resonant to the microwave mode. To quantify this influence, we should extend the multi-level JC model in the main text by considering the coupling between this spin level with the microwave mode. However, in the light that this coupling has no influence on the cooling dynamics and steady-state of the NV spin ensemble, we

conclude that this coupling affects only Eq. (20) for the intra-resonator photon number:

$$\langle \hat{a}^\dagger \hat{a} \rangle(t) \approx \frac{N(k_{eet}^{31} + k_{eet}^{21})\langle \hat{\sigma}_1^{11} \rangle(t) + \kappa n_m^{th}}{N \sum_{i=2,3} k_{eet}^{i1} [\langle \hat{\sigma}_1^{11} \rangle(t) - \langle \hat{\sigma}_1^{ii} \rangle(t)] + \kappa}, \tag{12}$$

where we have introduced the energy transfer rates $k_{eet}^{i1} = -2g_{i1}^2 \mathrm{Im}\tilde{\delta_{i1}}^{-1}$ with the complex detuning $\tilde{\delta}_{31} = (\omega_m - \omega_{31}) + i\left[(\kappa + k_{12} + k_{13} + k_{31})/2 + \xi + \chi_3\right]$ and $\tilde{\delta}_{21} = (\omega_m - \omega_{21}) + i\left[(\kappa + k_{13} + k_{12} + k_{21})/2 + \xi + \chi_2\right]$. Assuming the same parameters for the $-1 \to 0$ and $+1 \to 0$ transition, we can use the above expression to compute the intra-resonator photon number at steady-state as function of the microwave mode frequency ω_m for the laser excitation of power 2 W, see the Supplementary Figure 4. We see that the two spin transitions contribute together to the microwave mode cooling, and the off-resonant spin transition contributes to the microwave mode cooling by 5% when the other transition is resonant to the microwave mode. Note that the photon number decreases with increasing microwave mode frequency ω_m due to the dependence of the thermal photon number n_m^{th} on this frequency.

SUPPLEMENTARY NOTE 5: RATE EQUATIONS FOR MICROWAVE MODE COOLING

In this Supplementary Note, we explain how to derive the rate equations by ignoring the spin-spin correlation and eliminating the spin-photon correlation, and how to further simplify these equations by eliminating the population of triplet and singlet excited states, as well as how to obtain the analytical expressions for the steady-state of the NV spins-microwave resonator system.

Eliminate Spin-Photon Correlations

To clarify whether the collective coupling plays a role in the microwave mode cooling via the optically cooled NV spin ensemble, we derive the rate equations for the mean-field quantities given in the previous Supplementary Note. To this end, we assume the spin-spin correlations vanish, i.e. $\langle \hat{\sigma}_1^{31} \hat{\sigma}_2^{13} \rangle \approx 0$, and we solve Eq. (10) in steady-state

$$\langle \hat{a}^\dagger \hat{\sigma}_1^{13} \rangle \approx g_{31} \tilde{\delta}^{-1} \left[\langle \hat{\sigma}_1^{11} \rangle \langle \hat{a}^\dagger \hat{a} \rangle - \langle \hat{\sigma}_1^{33} \rangle \left(1 + \langle \hat{a}^\dagger \hat{a} \rangle\right) \right], \tag{13}$$

with the complex frequency detuning $\tilde{\delta} = (\omega_m - \omega_{31}) + i\left[(\kappa + k_{12} + k_{13} + k_{31})/2 + \xi + \chi_3\right]$. Inserting the above result into Eq. (9), we obtain

$$\partial_t \langle \hat{a}^\dagger \hat{a} \rangle \approx \kappa \left(n_m^{th} - \langle \hat{a}^\dagger \hat{a} \rangle\right) - N k_{eet} \langle \hat{\sigma}_1^{11} \rangle \langle \hat{a}^\dagger \hat{a} \rangle + N k_{eet} \langle \hat{\sigma}_1^{33} \rangle \left(1 + \langle \hat{a}^\dagger \hat{a} \rangle\right), \tag{14}$$

with the energy transfer rate $k_{eet} = -2g_{31}^2 \mathrm{Im}\tilde{\delta}^{-1}$ for single NV center to the microwave mode. If we ignore the spontaneous emission of microwave photon and consider that the imaginary part of $\tilde{\delta}$ is dominated by the photon damping rate κ and the spin dephasing χ_3, we will obtain Eq. (2) in the main text. Inserting Eq. (13) to Eqs. (2) and (4), we obtain

$$\begin{aligned} \partial_t \langle \hat{\sigma}_1^{11} \rangle \approx & -(k_{12} + k_{13} + \xi) \langle \hat{\sigma}_1^{11} \rangle + (\xi + k_{sp}) \langle \hat{\sigma}_1^{44} \rangle + k_{21} \langle \hat{\sigma}_1^{22} \rangle \\ & + k_{31} \langle \hat{\sigma}_1^{33} \rangle - k_{eet} \langle \hat{\sigma}_1^{11} \rangle \langle \hat{a}^\dagger \hat{a} \rangle + k_{eet} \langle \hat{\sigma}_1^{33} \rangle \left(1 + \langle \hat{a}^\dagger \hat{a} \rangle\right), \end{aligned} \tag{15}$$

$$\begin{aligned} \partial_t \langle \hat{\sigma}_1^{33} \rangle \approx & -\xi \langle \hat{\sigma}_1^{33} \rangle + (k_{sp} + \xi) \langle \hat{\sigma}_1^{66} \rangle + k_{73} \langle \hat{\sigma}_1^{77} \rangle + k_{13} \langle \hat{\sigma}_1^{11} \rangle \\ & - k_{31} \langle \hat{\sigma}_1^{33} \rangle + k_{eet} \langle \hat{\sigma}_1^{11} \rangle \langle \hat{a}^\dagger \hat{a} \rangle - k_{eet} \langle \hat{\sigma}_1^{33} \rangle \left(1 + \langle \hat{a}^\dagger \hat{a} \rangle\right). \end{aligned} \tag{16}$$

Eqs. (14), (15) and (16) together with Eqs. (3), (5)-(8) constitute the rate equations for the microwave mode cooling.

Our equations differ from those in Ref. [1] in the following aspects: (1) the energy transfer rate depends on the frequency detuning, and thus our rate equations can be also applied to the off-resonant case; (2) the energy transfer rate depends also on the resonator mode damping rate κ and the optical pumping rate ξ, and thus our equations are valid when these two rates become comparable with the spin-dephasing rate; (3) our equations account for the resonator-mediated spontaneous emission of microwave photon (i.e. superradiance) and thus are also valid when the microwave mode is cooled to the ground state. In the experiments reported in [1], the spin-dephasing rate dominates over other rates and the number of microwave photons is very large, and in this limit, our rate equations are equivalent to those developed in Ref. [1].

Eliminate Population of Higher Excited States

In light of Fig. 2a in the main text and the Supplementary Figure 2a, the population of the triplet and single excited state seems to follow adiabatically the population on the spin levels of the triplet ground state due to the large

spontaneous emission rate compared to other rates. Motivated by this, we might apply the adiabatic approximation to eliminate the population on the triplet and singlet excited states. To this end, we consider the steady-state solutions for these populations from Eqs. (5)-(8): $\langle\hat{\sigma}_1^{44}\rangle \approx \langle\hat{\sigma}_1^{11}\rangle\frac{\xi}{k_{sp}+\xi+k_{47}}$, $\langle\hat{\sigma}_1^{55}\rangle \approx \langle\hat{\sigma}_1^{11}\rangle\frac{\xi}{k_{sp}+\xi+k_{57}}$, $\langle\hat{\sigma}_1^{66}\rangle \approx \langle\hat{\sigma}_1^{11}\rangle\frac{\xi}{k_{sp}+\xi+k_{67}}$, and $\langle\hat{\sigma}_1^{77}\rangle \approx \frac{1}{k_{71}+k_{72}+k_{73}}(k_{47}\langle\hat{\sigma}_1^{44}\rangle + k_{57}\langle\hat{\sigma}_1^{55}\rangle + k_{67}\langle\hat{\sigma}_1^{66}\rangle)$, and insert these results into Eqs. (3), (15) and (16) to obtain

$$\begin{aligned}
\partial_t\langle\hat{\sigma}_1^{11}\rangle \approx& -(\tilde{k}_{11}+k_{12}+k_{13})\langle\hat{\sigma}_1^{11}\rangle + (\tilde{k}_{21}+k_{21})\langle\hat{\sigma}_1^{22}\rangle \\
&+ (\tilde{k}_{31}+k_{31})\langle\hat{\sigma}_1^{33}\rangle - k_{eet}\langle\hat{\sigma}_1^{11}\rangle\langle\hat{a}^\dagger\hat{a}\rangle + k_{eet}\langle\hat{\sigma}_1^{33}\rangle(1+\langle\hat{a}^\dagger\hat{a}\rangle), \qquad (17)\\
\partial_t\langle\hat{\sigma}_1^{22}\rangle \approx& -(\tilde{k}_{22}+k_{21})\langle\hat{\sigma}_1^{22}\rangle + (\tilde{k}_{12}+k_{12})\langle\hat{\sigma}_1^{11}\rangle + \tilde{k}_{31}\langle\hat{\sigma}_1^{33}\rangle, \qquad (18)\\
\partial_t\langle\hat{\sigma}_1^{33}\rangle \approx& -(\tilde{k}_{33}+k_{31})\langle\hat{\sigma}_1^{22}\rangle + (\tilde{k}_{13}+k_{13})\langle\hat{\sigma}_1^{11}\rangle \\
&+ \tilde{k}_{23}\langle\hat{\sigma}_1^{22}\rangle + k_{eet}\langle\hat{\sigma}_1^{11}\rangle\langle\hat{a}^\dagger\hat{a}\rangle - k_{eet}\langle\hat{\sigma}_1^{33}\rangle(1+\langle\hat{a}^\dagger\hat{a}\rangle). \qquad (19)
\end{aligned}$$

In the above equations, we have defined the rates

$\tilde{k}_{11} = \xi\frac{k_{47}}{k_{sp}+\xi+k_{47}}(1-\frac{k_{71}}{k_{71}+k_{72}+k_{73}})$	$\tilde{k}_{21} = \xi\frac{k_{57}}{k_{sp}+\xi+k_{57}}\frac{k_{71}}{k_{71}+k_{72}+k_{73}}$	$\tilde{k}_{31} = \xi\frac{k_{67}}{k_{sp}+\xi+k_{67}}\frac{k_{71}}{k_{71}+k_{72}+k_{73}}$
$\tilde{k}_{12} = \xi\frac{k_{47}}{k_{sp}+\xi+k_{47}}\frac{k_{72}}{k_{71}+k_{72}+k_{73}}$	$\tilde{k}_{22} = \xi\frac{k_{57}}{k_{sp}+\xi+k_{57}}(1-\frac{k_{72}}{k_{71}+k_{72}+k_{73}})$	$\tilde{k}_{32} = \xi\frac{k_{67}}{k_{sp}+\xi+k_{67}}\frac{k_{72}}{k_{71}+k_{72}+k_{73}}$
$\tilde{k}_{13} = \xi\frac{k_{47}}{k_{sp}+\xi+k_{47}}\frac{k_{73}}{k_{71}+k_{72}+k_{73}}$	$\tilde{k}_{23} = \xi\frac{k_{57}}{k_{sp}+\xi+k_{57}}\frac{k_{73}}{k_{71}+k_{72}+k_{73}}$	$\tilde{k}_{33} = \xi\frac{k_{67}}{k_{sp}+\xi+k_{67}}(1-\frac{k_{73}}{k_{71}+k_{72}+k_{73}})$

Here, $\tilde{k}_{ii}$ are the rates of the population transfer from the spin levels of the triplet ground state to the higher excited states, where $\tilde{k}_{ij}$ with $i \neq j = 1,2,3$ are the rates of the population transfer from the i-th spin level to the j-th spin level of the triplet ground state via the higher excited states.

Our calculations show that k_{eet} is on the order of 10^{-7} Hz while the other rates in the above equations are on the order of $10^2, 10^3$ Hz. Thus, in Eqs. (17) to (19), we can ignore the terms proportional to the photon number $\langle\hat{a}^\dagger\hat{a}\rangle$. Furthermore, the photon damping rate κ and the collective energy transfer rate Nk_{eet} are on the order of 10^6 Hz, which is orders of magnitude larger than the rates appearing in Eqs. (17) to (19) for the spin level populations. As a result, we might also apply the adiabatic approximation to Eq. (14) to obtain

$$\langle\hat{a}^\dagger\hat{a}\rangle(t) \approx \frac{Nk_{eet}\langle\hat{\sigma}_1^{11}\rangle(t) + \kappa n_m^{th}}{Nk_{eet}[\langle\hat{\sigma}_1^{11}\rangle(t) - \langle\hat{\sigma}_1^{33}\rangle(t)] + \kappa}. \qquad (20)$$

Analytical Expressions

Since the parameters related to the ±1 spin levels are similar, the equations for the populations $\langle\hat{\sigma}_1^{22}\rangle$ and $\langle\hat{\sigma}_1^{33}\rangle$ are equivalent, leading to $\langle\hat{\sigma}_1^{33}\rangle \approx \langle\hat{\sigma}_1^{22}\rangle \approx (1-\langle\hat{\sigma}_1^{11}\rangle)/2$. In this case, we can approximate Eq. (17) as

$$\partial_t\langle\hat{\sigma}_1^{11}\rangle \approx -(\tilde{k}_{11}+k_{12}+k_{13}+\tilde{k}_{31}+k_{31})\langle\hat{\sigma}_1^{11}\rangle + \tilde{k}_{31} + k_{31}, \qquad (21)$$

and solve it analytically to obtain

$$\langle\hat{\sigma}_1^{11}\rangle(t) \approx (c_1-c_0)e^{-(\tilde{k}_{11}+k_{12}+k_{13}+\tilde{k}_{31}+k_{31})t} + c_0. \qquad (22)$$

For the optical spin cooling period in the Supplementary Fig. 2(a), the two constants are $c_0 \approx \frac{\tilde{k}_{31}+k_{31}}{\tilde{k}_{11}+k_{12}+k_{13}+\tilde{k}_{31}+k_{31}}$ and $c_1 \approx 1/3$. For the thermalization period in the Supplementary Fig. 2, the effective rates are $\tilde{k}_{31} = \tilde{k}_{11} = 0$ and the constants are $c_0 \approx 1/3$ and $c_1 \approx \frac{k_{31}}{k_{12}+k_{13}+k_{31}}$. From this population we can compute the population of the ±1 spin levels $\langle\hat{\sigma}_1^{33}\rangle(t) \approx \langle\hat{\sigma}_1^{22}\rangle(t) \approx 1-2\langle\hat{\sigma}_1^{11}\rangle(t)$, as well as the intra-resonator photon number $\langle\hat{a}^\dagger\hat{a}\rangle(t) \approx \frac{Nk_{eet}\langle\hat{\sigma}_1^{11}\rangle(t)+\kappa n_m^{th}}{Nk_{eet}[\langle\hat{\sigma}_1^{11}\rangle(t)-\langle\hat{\sigma}_1^{33}\rangle(t)]+\kappa}$ with the energy transfer rate $k_{eet} = \frac{2g_{31}^2\chi}{(\omega_m-\omega_{31})^2+\chi^2}$, where $\chi = (\kappa+k_{12}+k_{13}+k_{31})/2 + \xi + \chi_3$ is the total dephasing rate. The photon number can be further simplified as $\langle\hat{a}^\dagger\hat{a}\rangle(t) \approx \frac{\kappa n_m^{th}}{Nk_{eet}[\langle\hat{\sigma}_1^{11}\rangle(t)-\langle\hat{\sigma}_1^{33}\rangle(t)]+\kappa}$ for $Nk_{eet} \ll \kappa n_m^{th}$. The above expressions indicate that the population of the 0 spin level evolves exponentially during both the optical cooling and thermalization period, and the intra-resonanter photon number behaves oppositely.

Finally, we derive analytical expressions for the steady-state situation. To this end, we ignore the coupling with the microwave mode in Eqs. (18) and (19), and consider the equations in steady-state. Using the relation $\langle\hat{\sigma}_1^{11}\rangle \approx 1-\langle\hat{\sigma}_1^{22}\rangle - \langle\hat{\sigma}_1^{33}\rangle$, we can solve these equations analytically and obtain $\langle\hat{\sigma}_1^{22}\rangle \approx \frac{B(\tilde{k}_{12}+k_{12})-C(\tilde{k}_{13}+k_{13})}{AB-CD}$, $\langle\hat{\sigma}_1^{33}\rangle \approx \frac{A(\tilde{k}_{13}+k_{13})-D(\tilde{k}_{12}+k_{12})}{AB-CD}$ with the abbreviations $A = \tilde{k}_{22}+k_{21}+\tilde{k}_{12}+k_{12}, B = \tilde{k}_{33}+k_{31}+\tilde{k}_{13}+k_{13}, C = \tilde{k}_{12}+k_{12}-\tilde{k}_{32}, D = \tilde{k}_{13}+k_{13}-\tilde{k}_{23}$. We have verified that these analytical expressions reproduce the results obtained with the rate equations.

SUPPLEMENTARY NOTE 6: COUNTERACTING OPTICAL HEATING OF DIAMOND

The results in the main text show that a laser power about 1 W is sufficient to achieve the microwave mode cooling and observe C-QED effects at room temperature, while a laser power about 100 W is necessary to achieve optimal spin cooling, and thus much better performance. Under such strong laser illumination, the diamond sample might be overheated. It was reported in the experiment of the diamond maser at room temperature [2] that the temperature increases by 35 K when the laser power increases to 0.4 W, suggesting the relationship $\Delta T/\Delta P = 87.5$ K/W. According to Ref. [14], the change of the zero-field splitting depends on the temperature change as $\Delta D/\Delta T = -2\pi\times 0.074$MHz/K.

Assuming similar properties of the diamond sample in our study, we expect that for the laser power $P = 1$ W, the temperature raises by 87.5 K, and the frequency drifts by $-2\pi \times 6.48$ MHz. This simple calculation indicates that we must mitigate the effects of optical heating. To counteract the optical heating, we can cool the diamond sample with heat-sinking, forced air, immersive liquid cooling or heat pipes, as pointed out in Ref. [1]. As an example, in the experiment [15], it was demonstrated that by cooling the diamond sample with water and N_2 gas, the temperature rise can be managed within 30 K for a laser power up to 24 W. If this cooling is still efficient for much higher laser power, we expect a temperature rise of 125 K for a 100 W laser power, and a frequency drift of $2\pi \times 9.25$ MHz. This is acceptable, and if necessary, the frequency drift can be counteracted by a Zeeman shift induced by a magnetic field.

The temperature discussed above refers to that of the diamond lattice phonons T_{lat} not the NV spins and the microwave mode, and it affects the phenomena studied in the main text only by increasing the spin-lattice relaxation rate. According to Refs. [5, 6], for lattice temperatures above 200 K, the spin-lattice relaxation rate is determined by the two-phonon Raman process, and scales as $k_{i1} \propto T_{lat}^5$ with temperature. As a result, we have $k_{i1} \approx k_{1i}$ $(i = 2, 3)$ to $k_{i1} \times [(T_{ini} + \Delta T)/T_{ini}]^5$ with $T_{ini} = 293$ K and $\Delta T = 125$ K. For the high frequency resonator, $k_{31} \approx k_{21}$ increases from 208 Hz to 2181 Hz. For the lower frequency resonator, $k_{31} \approx k_{21}$ increases from 83 Hz to 490 Hz. Even with the increased spin-lattice relaxation rate, we can still obtain results as in the main text except that the laser power should be increased slightly to counteract the increased spin-lattice relaxation rate.

SUPPLEMENTARY REFERENCES

[1] Ng, W., Wu, H. & Oxborrow, M. Quasi-continuous cooling of a microwave mode on a benchtop using hyperpolarized NV^- diamond. *Appl. Phys. Lett.* **119**, 234001 (2021).

[2] Breeze, J. D. et al. Continuous-wave room-temperature diamond maser. *Nature* **555**, 493-496 (2018).

[3] Wu, H. et al. Room-Temperature quasi-continuous-wave pentacene maser pumped by an invasive Ce : YAG luminescent concentrator. *Phys. Rev. Applied* **14**(6), 64017 (2020).

[4] Clevenson, H. et al. Broadband magnetometry and temperature sensing with a light-trapping diamond waveguide. *Nat. Phys.* **11**, 393-397 (2015).

[5] Norambuena, A. et al. Spin-lattice relaxation of individual solid-state spins. *Phys. Rev. B* **97**, 94304 (2018).

[6] Jarmola, A. et al. Temperature- and magnetic-field-dependent longitudinal spin relaxation in nitrogen-vacancy ensembles in diamond. *Phys. Rev. Lett.* **108**, 197601 (2012).

[7] Mrózek, M. et al. Longitudinal spin relaxation in nitrogen-vacancy ensembles in diamond. *EPJ Quantum Technol.* **2**, 22 (2015).

[8] Ivády, V. Longitudinal spin relaxation model applied to point-defect qubit systems. *Phys. Rev. B* **101**, 155203 (2020).

[9] Barry, J. F. et al. Sensitivity optimization for NV^- diamond magnetometry. *Rev. Mod. Phys.* **92**, 015004 (2020).

[10] Edmonds, A. M. et al. Characterisation of CVD diamond with high concentrations of nitrogen for magnetic-field sensing applications. *Mater. Quantum Technol.* **1**, 025001 (2021).

[11] Putz, S. et al. Protecting a spin ensemble against decoherence in the strong-coupling regime of cavity QED. *Nat. Phys.* **10**, 720-724 (2014).

[12] Kubo, Y. et al. Strong coupling of a spin ensemble to a superconducting resonator. *Phys. Rev. Lett.* **105**, 140502 (2010).

[13] Oshnik, N. et al. Robust magnetometry with single NV centers via two-step optimization. *Phys. Rev. A* **106**, 013107 (2022).

[14] Acosta, V. M. et al. Temperature dependence of the nitrogen-vacancy magnetic resonance in diamond. *Phys. Rev. Lett.* **104**, 70801 (2010).

[15] Sarkar, A. et al. Rapidly enhanced spin polarization injection in an optically pumped spin ratchet. *Phys. Rev. Applied* **18**, 034079 (2022).